RSC Advances

PAPER

View Article Online
View Journal | View Issue

Cite this: *RSC Adv.*, 2024, **14**, 7910

AIE/AEE tripodal PEGyl-melphalan supramolecules and detection of trinitrophenol in water†

Zhenghua Zhang,*[a] Yonghe Zhang,[a] Liyan Cheng,[a] Fei Wen,[a] Dan Feng,[a] Feng Zhou,[a] Yu-Hua Shi[b] and Weibing Xu *[c]

Received 24th October 2023
Accepted 15th February 2024

DOI: 10.1039/d3ra07252e

rsc.li/rsc-advances

Herein, the design of a novel aggregation-induced emission (AIE) supramolecular fluorescence sensor (TA-PEG*n*) based on a tridentate melphalan derivative and three different molecular weight PEGs is presented. The three TA-PEG*n* sensors could self-assemble into a supramolecular system in water and show sensitive and selective responses toward trinitrophenol.

Introduction

Over 30% of the water worldwide is polluted by organic compounds (OCs). Thousands of people die from various diseases caused by organic compounds polluting water.[1] Among OCs, 2,4,6-trinitrophenolare (PA) is the most dangerous and notorious because it is toxic, posing tremendous risks to human health, and it is widely used in dye and pharmaceutical industries.[2] The natural degradation of PA is very difficult because of its electron-deficient character, which is related to the strong electron-withdrawing ability of nitro groups. PA is a strong organic acid ($pK_a = 0.38$) and can easily enter water and soil due to its good water solubility. PA is a strong irritant to the skin/eyes and causes potential damage to organs involved in the respiratory system and liver when it comes in contact with the human body.[3] Therefore, it is urgent to achieve rapid and accurate detection of PA in water. Various methods, including GC-MS, HPLC, surface-enhanced Raman, and sensors, have been developed and built to detect PA.[4–6] Most available methods are expensive and overly sophisticated for wide applications. Fluorescence-based sensing methods stand out among various techniques due to their simplicity, high sensitivity, affordability, straightforward sample preparation, and portability, offering immense potential.[7] Lots of fluorescent sensors have been constructed to detect PA.[8–10] A donor–acceptor conjugated polymer based on diethylamine phenyl and benzothiadiazole groups was fabricated to detect PA with a K_{sv} constant of 1.8×10^3 M^{-1}.[11] Hyperbranched conjugated polymers (HCPs) were first synthesized using truxene and diethynylbenzene derivates, which were carried by F127 in water to form highly fluorescent HCP micelles. The limit of detection for PA was about 2.8×10^{-7} mol L^{-1}.[12] The concept of aggregation-induced emission (AIE) was proposed by Tang's research group several decades ago based on their discovery that 1-methyl-1,2,3,4,5-pentaphenylsilole (HPS) exhibited negligible fluorescence in acetonitrile solution but showed significant enhancement of fluorescence upon the addition of water.[13] This finding led to the development of the AIE concept. This phenomenon stands in stark contrast to the phenomenon of aggregation-caused quenching (ACQ). Essentially, AIE describes a fluorescence phenomenon in which molecules in an aggregated state exhibit stronger fluorescence emission compared to individual molecules.[14,15] This is due to the restriction of intramolecular rotation. AIE has found extensive applications in the fields of fluorescence sensing, biosensing and cellular imaging.[16] A highly efficient and selective chemosensor for the detection of trace PA was designed and synthesized utilizing a quinoxaline derivative as the sensing component.[17] Building upon our previous research on fluorescence chemosensors, we developed a PEG-based fluorescent probe with excellent AIE properties and water solubility in this study.

The identification efficiency of picric acid in aqueous solution was investigated.

Results and discussion

First, a chlorination reaction was carried out using 1 equivalent of benzoyl chloride and 3 equivalents of mefenamic acid to construct the triadic core structure. Next, through a reaction between the

[a]*Yellow River Basin Ecotope Integration of Industry and Education Research Institute, Lanzhou Resources & Environment Voc-Tech University, Lanzhou 730022, China. E-mail: zhangzhenghua1021@163.com*

[b]*WuWei JinCang Bioscience Co., Ltd, Hongshagang Chemical Industrial Park, Wuwei 733000, China*

[c]*College of Science, Gansu Agricultural University, Lanzhou 730000, China. E-mail: xuwb@gsau.edu.cn*

† Electronic supplementary information (ESI) available: The experimental part, MALDI-TOF mass spectrum, fluorescence emission spectra of TA-PEG-5 and 2 in pure water and the CAC values of TA-PEG-0.75; fluorescent emission spectra of fluorescence titration and linear fitting of TA-PEG-5, 2 and 0.75 by addition of various concentrations of PA; quenching efficiencies and nonlinear curve fitting of TA-PEG-5, 2 and 0.75 in the presence of different concentrations of PA; fluorescence intensity of TA-PEG-5, 2 and 0.75 to PA in the presence of various nitroaromatic compounds; fluorescence intensity of TA-PEG*n* in different pH; IR spectra, fluorescence lifetime spectra; the partial ^{1}H NMR spectra and SEM images; UV intensity of TA-PEG*n* solution, free PA (1.0 & KHgr; 10^{-3} mol L^{-1}) and mixture solution; Fluorescence images of TA-PEG*n*-PVA film. See DOI: https://doi.org/10.1039/d3ra07252e

carboxyl group in mefenamic acid molecules and hydroxyl groups on polyethylene glycol, water-soluble and non-toxic polyethylene glycol was linked to the core, simultaneously restricting the free rotation of the carboxyl groups within core molecules. This resulted in the successful assembly of a supramolecular self-assembling system designed with three-footed moieties and aggregation-induced luminescent units. The typical fabrication route is depicted in Scheme 1. MALDI-TOF analyses of the three conjugates showed a single series of molecular weights. The number-averaged molecular weights of the conjugate are ~3250, 7830 and 16 520 amu. This suggests that conjugates were successfully constructed (Fig. S1a–c†). The long PEG chains in TA-PEG5 and TA-PEG2 increase their hydrophilicity, so they can be completely dissolved in water. Therefore, TA-PEG0.75 was selected as a representative compound for deep exploration of the aggregation-induced emission (AIE) properties. H_2O, DMSO, DMF, EtOH, CH_3CN, DCM and $CHCl_3$ are the seven regularly used solvents that were chosen to explore how different solvents affect the fluorescence emission of TA-PEG0.75. The results are shown in Fig. 1a. TA-PEG0.75 is insoluble in H_2O, EtOH and CH_3CN and has the highest relative fluorescence emission intensity in DMSO. An optimal excitation wavelength optimization experiment was carried out in DMSO solution at a concentration of 2×10^{-5} M, and the results are shown in Fig. 1b. It can be seen that the compounds have the strongest fluorescence emission at 470 nm excitation, which was selected as the optimal excitation wavelength. The fluorescence emission curves of TA-PEG-5 and 2 were evaluated in pure water at same concentrations and excitation wavelength (Fig. S2a†). It can be found that the fluorescence emission intensity of TA-PEG5 is greater than that of TA-PEG2 at the same concentration in water, which may be related to the long PEG chain. To investigate the aggregation-induced emission (AIE) properties of TA-PEG0.75, detailed studies were conducted based on ultraviolet-visible absorption spectra, fluorescence emission spectra, critical aggregation concentration (CAC), and scanning electron microscopy images. As shown in Fig. 1c, the compounds exhibited broad absorption capabilities in the wavelength range of 200–550 nm in DMSO. The absorption intensity increased with increasing concentration, while the shape of curves remained consistent, indicating its dependence on concentration. Fluorescence emission spectra at different concentrations were measured as shown in Fig. 1d. It can be observed that it exhibited weak fluorescence emission at low concentrations, and the fluorescence intensity gradually increased with increasing concentration. This may be attributed to the AIE phenomenon resulting from the self-assembly. Additionally, the CAC value of TA-PEG0.75 was calculated to be 0.049 mg mL^{-1} (Fig. S2b†). Subsequently, the AIE properties of TA-PEG0.75 were further investigated in a binary solvent system comprising DMSO and water. As shown in Fig. 1e and f, the fluorescence intensity gradually increases with the increase of the water content. When the water content in the solution increased to 99%, the fluorescence intensity reached the maximum, and no precipitation occurred. This result further indicates that TA-PEG0.75 has AIE characteristics. AIE, which stands for aggregation-induced emission, refers to the phenomenon where a substance emits little-to-no fluorescence in a dispersed solution, but the emission intensity increases in the aggregated state. Since TA-PEG5 and TA-PEG2 are completely soluble in water and their aqueous solutions inherently exhibit fluorescence properties, it was not possible to assess their AIE properties in a binary solvent system. To further compare the fluorescence performance of TA-PEG*n*, quinine sulfate was used as a reference, and fluorescence quantum yields were calculated using eqn (S1).†[18] The fluorescence quantum yields (Φ) of TA-PEG5, 2 and 0.75 are 81.1%, 76.9% and 34.7%, respectively. It can be seen that the fluorescence quantum yields increase with the elongation of the PEG chain. Φ quantifies the fluorescence emission efficiency, with higher values indicating stronger fluorescence emission capability.[19]

The experiment that TA-PEG*n* can be used as a fluorescent probe to identify picric acid was carried out in pure water, because TA-PEG5 and 2 have good fluorescence properties in aqueous solution, and it is convenient to detect the presence of picric acid in the pure water phase. As shown in Fig. S3,† a series of nitro-aromatic compounds (NACs, 52 eq. mol), including picric acid (PA), 2-nitrophenol, 3-nitrophenol, 4-nitrophenol, 2,4-dinitrophenol, 2-nitrobenzoic acid, 3-nitrobenzoic acid, 4-nitrobenzoic acid, 4-nitrobenzaldehyde, 2-nitroaniline, 3-nitroaniline, 4-nitroaniline, 4-chloronitrobenzene and 4-nitrotoluene, were added into an aqueous solution of TA-PEG5 (2×10^{-5} M), respectively. In this context, the addition of the PA compound to the solution results in the complete quenching of fluorescence, whereas there is no discernible change in the fluorescence of other solutions. The same exact fluorescence quenching was also observed in TA-PEG2 and 0.75 solutions. TA-PEG0.75 is dissolved in a DMF/H_2O (1 : 99, v/v) binary solution with a concentration of 2×10^{-5} M. It can be seen that TA-PEG5, 2 and 0.75 can selectively recognize PA in a mixture of various nitro-aromatic compounds, showing excellent selective recognition characteristics. To explore the fluorescence recognition characteristics of TA-PEG*n* for PA, the fluorescence titration experiment of TA-PEG*n* and PA was first carried out, as shown in Fig. S4a–c.† The intense fluorescence emission spectrum of TA-PEG-5000 was quenched with the gradual increase of PA (0–52 equivalent). Highly similar fluorescence quenching behaviour was also observed in solutions of TA-PEG2 and TA-PEG0.75. The fluorescent titration curves of PA with TA-PEG5, 2, and 0.75 exhibited excellent linearity, as depicted in Fig. S4d–f.† By employing 3σ/s as the basis,[20,21] detection limits for PA were determined to be 5.7×10^{-7} M, 1.1×10^{-6} M, and 1.8×10^{-6} M for TA-PEG5, 2, and 0.75, respectively, where σ represents the standard deviation of blank measurements and *s*

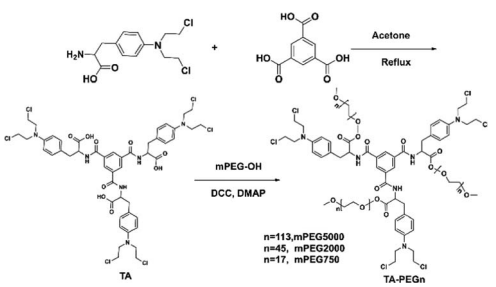

Scheme 1 Schematic illustration of the fabrication of TA-PEG*n*.

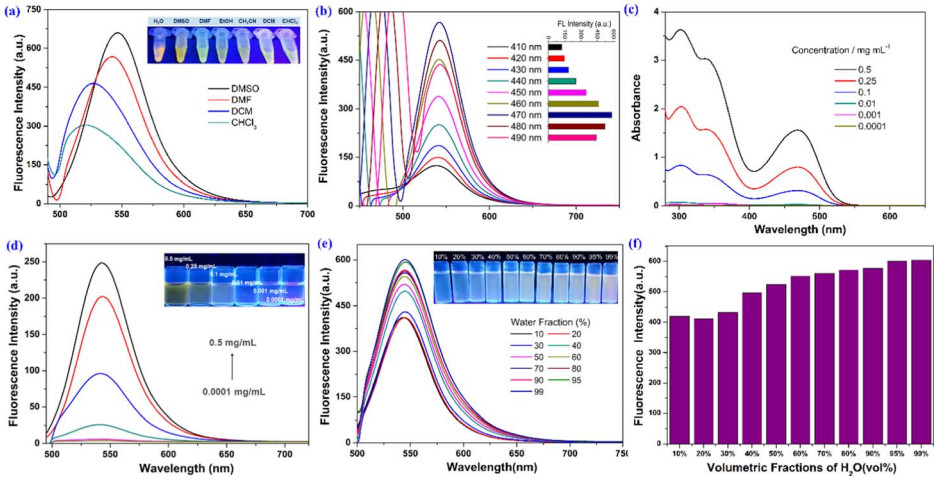

Fig. 1 Fluorescence emission spectra under different solvents (a) and different excitation wavelengths (b), UV-vis (c) and fluorescence emission (d) at different concentrations, and fluorescence emission curves (e) and intensity (f) of TAPEG0.75 in DMF/H_2O solution.

denotes the slope. Upon comparison, it can be observed that TA-PEG5, with the longest PEG chain, exhibited the lowest limit of detection (LOD), indicating higher sensitivity compared to the other two compounds with shorter PEG chains. The magnitude of the quenching coefficient (K_{SV}) can indicate the strength of the interaction between TA-PEG*n* and PA. Through a fluorescence titration experiment, it can be calculated according to the Stern–Volmer (SV) equation: $F_0/F = 1 + K_{SV}[G]$,[22] where F_0 represents the fluorescence intensity of TA-PEG*n* in the absence of PA. F represents the fluorescence intensity in the presence of PA; [G] is the molar concentration of PA. Fig. S5a–c† show the SV graphs of TA-PEG5, TA-PEG2 and 0.75 at different PA concentrations. The corresponding K_{SV} values between the three compounds and PA were 2.5×10^3 M^{-1}, 1.9×10^3 M^{-1} and 2.3×10^3 M^{-1}, respectively. It can be seen that the value does not change significantly with the chain length of PEG, indicating that the PA recognition ability of the three conjugates may not be directly related to the length of the PEG chain. Due to the direct correlation between the strength of interactions between TA-PEG*n* and PA and stability of complex formation, further investigation was conducted to determine respective binding constants (K_a) between TA-PEG*n* and PA. The value was obtained by the fluorescence titration experiment and calculated according to the nonlinear curve fitting method. $\Delta I = (\Delta I_\infty/[H_0])(0.5[G] + 0.5([H_0] + 1/K_a) - (0.5([G]^2 + (2[G](1/K_a - [H_0])) + (1/K_a + [H_0])^2)^{0.5}))$, where ΔI represents the change of fluorescence intensity of TA-PEG*n* at different concentrations of PA. ΔI_∞ represents the change of fluorescence intensity when TA-PEG*n* and PA are completely combined. $[H_0]$ represents the initial concentration of TA-PEG-*n*; [G] indicates the concentration of PA.[23] As shown in Fig. S5d–f,† the K_a values of TA-PEG5, 2 and 0.75 and PA are calculated by nonlinear fitting to be 3.2×10^4 M^{-1}, 2.2×10^4 M^{-1} and 6.4×10^3 M^{-1}, respectively. Compared to TA-PEG0.75, which has the shortest PEG chain, TA-PEG5 and TA-PEG2 exhibit a higher K_a with PA. This indicates that compounds with long PEG chains have stronger binding ability to PA, and long PEG chains are more conducive to forming stable complexes with PA. The anti-interference experiment of fluorescence probe TA-PEG*n* for PA selective recognition was further studied by a control experiment under competitive conditions. As shown in Fig. S6,† a large number of co-existing NACs do not cause any significant interference to the recognition of PA, indicating that there is no competitive recognition relationship between them. It was further confirmed that the three compounds showed highly specific recognition ability for PA. The recognition parameters of the three compounds for PA are summarized in Table S1.† The influence of pH on the fluorescence intensity and recognition performance of the three couplings was explored (Fig. S7a–c†). It can be seen that the fluorescence intensity of the three compounds hardly changed significantly as the pH value of the solution increased from 4 to 10. When 40 eq. PA solution was added, the fluorescence of the three compounds was basically quenched at different pH values, indicating that the fluorescence recognition performance was almost not affected by pH. This may be caused by the unique core–shell structure of TA-PEG*n*,[24] and it being difficult for a change of pH value to cause a change of hydrophobic nuclei in the conjugates. In addition, a comparison of TA-PEG*n* with literature reported chemosensors for PA is summarized in Table S2.† It can be found that the detection performance of the sensor reported in this study is better than that of some materials reported in the literature, which indicates that it has a considerable sensitivity to PA.

The PA response mechanism of the TA-PEG*n* compounds was investigated using ^1H NMR titration, infrared spectroscopy, and scanning electron microscopy (SEM) techniques. The infrared spectra of PA, TA-PEG*n* and TA-PEG*n* + PA are shown in Fig. S8.† For pure PA, the stretching vibration absorption peak of –OH appears at 3102 cm^{-1}. The symmetric and antisymmetric stretching vibration absorption peaks of =C–H on the benzene ring appear at 2972 and 2867 cm^{-1}.[25] The absorption band at 1338 cm^{-1} is assigned to the N–O symmetric stretching vibration of $-NO_2$ groups on PA molecules. The antisymmetric stretching vibration of $-NO_3$ groups can be found at 1638 cm^{-1}.[26] In TA-PEG*n*, $-CH_2-$ signal peaks appear at 2880 cm^{-1}, while signals at 1721 and 1520 cm^{-1} are

characteristic absorption peaks of C=O and benzene rings. Due to the coverage of the PEG long chains, the intensity of these signal peaks in TA-PEG2 and 5 is significantly lower than that in TA-PEG0.75. The O–H stretching vibration of free PA almost disappears, and the vibration of free PA at 2972 and 2867 cm^{-1} showed a red shift to 2936 and 2849 cm^{-1} when it formed a complex with TA-PEG-*n*. The absorption band at 1721 cm^{-1} on TA-PEG*n* exhibits a shift to a lower wavenumber (1702 cm^{-1}). The results indicate that –OH and benzene ring groups interact with TA-PEG-*n* during the recognition. In the ^{1}H NMR titration experiments (Fig. 2 and S9†), the signals of H1 on the –Cl–CH_2– group of TA-PEG-*n* showed a distinct downfield shift with the addition of different equivalents of PA solution, which indicated that H1 formed stable intermolecular hydrogen bonds with –OH on the PA molecules.[27] Meanwhile, –N–CH_2– protons (H2) on TA-PEG*n* showed slight upfield shifts. This may be assigned to H1 forming stable intermolecular hydrogen bonds with electron-rich –NO_2 on the PA molecules. Interestingly, hydrogen (H_a) in the benzene ring in PA, which is already in an electron-deficient state due to the electron-absorbing action of the three nitro groups, continues to move downfield with the increase of its content, which indicates that the electron-deficient state in PA is further intensified after the formation of TA-PEG*n*. This result indicated that the H_a forms hydrogen bond interactions with the chlorine atom on TA-PEG*n*.[28] The three PEG compounds with different chain lengths showed the same chemical shift of the hydrogen atoms in the NMR titration spectra of PA, and their recognition mechanism of PA was consistent. At the same time, it cannot be ignored that the unique semi-closed spatial structure of –N–$(CH_2CH_2Cl)_2$ also plays an irreplaceable role in this unique recognition mechanism. The intermolecular recognition model between PA and TA-PEG*n* is shown in the graphical abstract. These results indicate that the mechanism of fluorescence quenching caused by the formation of a new complex between PA and TA-PEG*n* is consistent with the static quenching mechanism. For further verification, the fluorescence lifetime of pure TA-PEG*n* solution without and with PA solution was investigated (Fig. S10a–f†). It can be seen that the fluorescence lifetime of the three solutions is almost not affected by the PA solution. Moreover, the addition of PA caused the micro-morphology of TA-PEG5, 2 and 0.75 to change into irregular rod-like particles, columnar structures, and nanoparticles (Fig. S11†), respectively. These morphological alterations unmistakably show that TA-PEG*n* and PA form a stable complex, in contrast to the morphology of free TA-PEG*n*. To further confirm the recognition mechanism, the UV absorption curves of pure TA-PEG*n*, PA and their mixed solutions were tested (Fig. S12a–c†). The maximum absorption wavelength of free PA is located at 365 nm, and the three couplings also have obvious absorption peaks at this wavelength (yellow arrow). There is a large overlap between two spectra at this wavelength, which is consistent with the fluorescence quenching mechanism of the inner filter effect. Meanwhile, the absorption peaks of the three couplings at 470 nm completely disappeared in the mixed solution (red arrow). Based on this, it can be concluded that the quenching mechanism caused by PA includes static quenching and the inner filter effect.

PA in deionized water and tap water samples were respectively determined by the three conjugates used in this study, as shown in Fig. S13a–c.† Tap water does not require any treatment. It can be found that the fluorescence emission intensity of the three conjugates in tap water is reduced to a negligible degree compared with that in deionized water. More interestingly, when 40 eq. PA is added, the fluorescence reduction degree of the three samples is almost the same in tap water and deionized water, indicating that the analytical method based on fluorescence quenching for PA detection in this study has good practical sample application value. PVA films containing the three conjugates were successfully prepared and used for PA recognition, as shown in Fig. S14a–f.† The pure film showed bright yellow illumination and after PA addition the film showed fluorescence quenching. This suggests that the TA-PVA film can be used to visually detect PA.

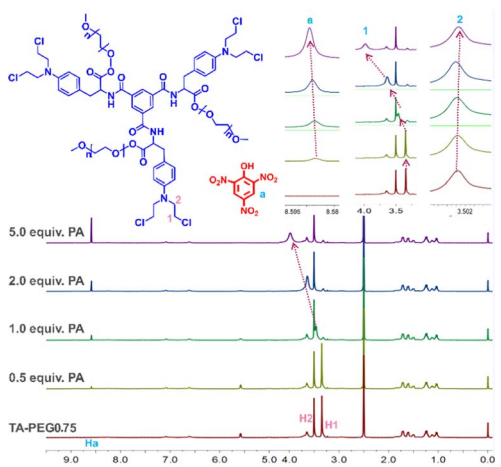

Fig. 2 Partial ^{1}H NMR spectra of TA-PEG0.75 (DMSO-d6) in the presence of varying amounts of PA.

Conclusions

In conclusion, fluorescent probe TA-PEG*n* with a tripod structure and different PEG chains was successfully constructed by precise design. The introduction of the PEG chain not only improves the water solubility of the compound but also endows the system with AIE characteristics. The TA-PEG*n* could act as a fluorescent sensor for rapid and selective detection of PA with high selectivity and sensitivity. The quenching mechanism caused by PA includes static quenching and the inner filter effect. It was found that with the increase of the PEG molecular weight, TA-PEG5 has the best fluorescence performance and highest selectivity and sensitivity to PA.

Conflicts of interest

There are no conflicts to declare.

Acknowledgements

The authors acknowledge the support of Gansu Province University Youth Doctoral Support Project (No. 2023QB-023 and 2023QB-022), Gansu Provincial Higher Education Innovation

Fund Project (No. 2023A-221, 2023A-222, 2023A-223), the Yellow River Basin Ecotope Integration of Industry and Education R&D Fund (No. XHYF2023-08, X2023A-12) of Lanzhou Resources & Environment Voc-Tech University, the Young Talent Innovation Project of Lanzhou City (No. 2023-QN-59) and the Youth Mentor Fund (GAU-QDFC-2023-06) of Gansu Agricultural University.

Notes and references

1 G. D. Liang, F. Ren, H. Y. Gao, Q. Wu, F. M. Zhu and B. Z. Tang, *ACS Sens.*, 2016, **1**, 1272–1278.
2 X. D. Zhang, G. J. Ren, M. L. Li, W. T. Yang and Q. H. Pan, *Cryst. Growth Des.*, 2019, **19**, 6308–6314.
3 S. Dhiman, N. Singla, M. Ahmad, P. Singh and S. Kumar, *J. Mater. Adv.*, 2021, **2**, 6466–6498.
4 R. G. Ewing, D. A. Atkinson, G. Eiceman and G. J. Ewing, *Talanta*, 2001, **54**, 515–529.
5 M. Godejohann, A. Preiss, K. Levsen and G. Wünsch, *Chromatographia*, 1996, **43**, 612–618.
6 J. Huang, L. Wang, C. Shi, Y. Dai, C. Gu and J. J. Liu, *Sens. Actuators, B*, 2014, **196**, 567–573.
7 W. T. Li, Z. J. Hu, J. Meng, X. Zhang, W. Gao, M. L. Chen and J. H. Wang, *J. Hazard. Mater.*, 2021, **411**, 125021.
8 J. Harathi and K. Thenmozhi, *Chemosphere*, 2022, **286**, 131825.
9 V. Saini, A. Gupta, K. Rangan and B. Khungar, *Dyes Pigm.*, 2020, **180**, 108447.
10 X. Jiao, H. Li and X. Cheng, *Mater. Today Chem.*, 2021, **22**, 100615.
11 B. Xu, X. Wu, H. Li, H. Tong and L. Wang, *Macromolecules*, 2011, **44**, 5089–5092.
12 W. Huang, E. Smarsly, J. Han, M. Bender, K. Seehafer, I. Wacker, R. R. Schröder and U. H. Bunz, *ACS Appl. Mater. Interfaces*, 2017, **9**, 3068–3074.
13 J. Luo, Z. Xie, J. W. Lam, L. Cheng, H. Chen, C. Qiu, H. S. Kwok, X. Zhan, Y. Liu and D. Zhu, *Chem. Commun.*, 2001, 1740–1741.
14 H. B. Wan, Q. F. Xu, P. Y. Gu, H. Li, D. Y. Chen, N. J. Li, J. H. He and J. M. Lu, *J. Hazard. Mater.*, 2021, **403**, 123656.
15 D. X. Li, D. Li, L. Zong, Y. H. Xiao, S. H. Sui, B. Zhuang, R. Li, H. L. Zhen, J. Li, Z. P. Huang, Z. G. Jiang and W. H. Wu, *Chem. Commun.*, 2022, **58**, 5296–5299.
16 F. Würthner, *Angew. Chem., Int. Ed.*, 2020, **59**, 14192–14196.
17 L. Y. Wang, M. M. Cui, H. Tang and D. R. Cao, *Dyes Pigm.*, 2018, **155**, 107–113.
18 L. L. Tong, X. X. Wang, Z. Z. Chen, Y. H. Liang, Y. P. Yang, W. Gao, Z. H. Liu and B. Tang, *Anal. Chem.*, 2020, **92**, 6430–6436.
19 A. Z. Tan, G. H. Yang and X. J. Wan, *Spectrochim. Acta, Part A*, 2021, **253**, 119583.
20 Z. H. Zhang, Y. M. Zhang, X. T. Kan, Q. Y. Yang, Y. J. Li, T. B. Wei, H. Yao and Q. Lin, *Dyes Pigm.*, 2021, **191**, 109389.
21 Y. J. Li, Y. F. Zhang, Y. M. Zhang, Z. H. Wang, H. L. Yang, H. Yao, T. B. Wei and Q. Lin, *Dyes Pigm.*, 2020, **181**, 108563.
22 M. H. Gehlen, *J. Photochem. Photobiol., C*, 2020, **42**, 100338.
23 Y. Tian, R. N. Hua, J. C. Yu, J. S. Sun and B. J. Chen, *Mater. Chem. Phys.*, 2012, **133**, 617–620.
24 F. F. Zhang, Y. Y. Chen, D. Zhang, Y. Jia, J. S. Meng, L. R. Jiang and S. K. Yang, *Int. J. Anal. Chem.*, 2022, **2022**, 6970747.
25 J. Zhang, X. Y. Li, X. P. Sun, Y. H. Liu, J. C. Hao, Y. B. Tan and A. X. Song, *New J. Chem.*, 2019, **43**, 18331–18338.
26 Y. L. Tang, H. F. Wu, J. M. Chen, J. L. Jia, J. P. Yu, W. Xu, Y. Y. Fu, Q. G. He, H. M. Cao and J. G. Cheng, *Dyes Pigm.*, 2019, **167**, 10–15.
27 M. B. Ahmed, J. L. Zhou, H. H. Ngo, M. A. H. Johir, L. Sun, M. Asadullah and D. Belhaj, *J. Hazard. Mater.*, 2018, **360**, 270–278.
28 X. Qu, L. Xiao and D. Q. Zhu, *J. Environ. Qual.*, 2008, **37**, 824–829.